A comparison between wave propagation in water-saturated and air-saturated porous materials[a)]

Donald G. Albert
US Army Cold Regions Research and Engineering Laboratory, 72 Lyme Road, Hanover, New Hampshire 03755-1290

(Received 29 July 1992; accepted for publication 24 September 1992)

The classical Biot theory [J. Acoust. Soc. Am. **28**, 168 (1956)] predicts the existence of three waves that can propagate in a fluid-saturated porous material: A fast compressional wave, a slow compressional wave, and a shear wave. Through use of this theory, propagation characteristics within water-filled and air-filled materials were compared in the 10 Hz–100 kHz band. Numerical calculations show that the ratio of fluid to solid motion for the slow compressional wave is around 2 in water-filled sand, but greater than 300 in air-filled sand. In addition, calculations of plane wave transmission from a fluid into a fluid-saturated porous solid were investigated. The calculations show that when the fluid is water, nearly all of the incident energy is transferred to the reflected wave and to the transmitted fast compressional wave that is traveling mainly in the solid frame. Only a slight frequency dependence occurs in the energy transfer. When the fluid is air, however, the interaction of the waves with the boundary becomes strongly dependent upon frequency, and most of the incident energy is transferred to the reflected wave and to the transmitted slow compressional wave traveling mainly in the pores. These theoretical results justify the different approaches used to treat reflections from porous materials in underwater and aeroacoustics. For reflections, air-filled soil or snow can be approximately modeled as a modified fluid (ignoring motion in the frame) rather than as a viscoelastic solid (ignoring motion in the pores), the approximation commonly used to model saturated undersea sediments.

I. INTRODUCTION

Although elastic or viscoelastic wave theory has proved to be very useful for many applications in seismology and acoustics, there are problems involving porous materials where such treatment is not appropriate, and consideration must be given to both the fluid and solid phases of the material. Biot[1–3] developed a theory of wave propagation based upon a macroscopic averaging that allows calculations to be made for porous materials.

In Biot's theory, the porous material is treated as a solid frame or matrix filled with a viscous fluid. By examining the coupling between the two phases and by averaging over a volume containing many pores. Biot derived constitutive equations governing this material. The volume average limits the theory to wavelengths that are much greater than the pore size, which is the case considered here. These constitutive equations were used to examine small amplitude motions; solutions from the resulting wave equations correspond to two compressional waves and one shear wave propagating in the porous material. For all three of these waves, the motion of the fluid and solid phases are coupled.

Biot's theory has been previously applied to two distinct applications that will be discussed and compared in this article. The first application is to wave propagation and attenuation in undersea sediments, which has been investigated by a number of researchers.[4–11] The second application is to problems in aeroacoustics and acoustic-to-seismic coupling.[12–17] The porous material is saturated with water in the first case and with air in the second. The differences in the two cases are caused mainly by the contrast in the fluid bulk modulus relative to the frame bulk and shear moduli, and will be discussed later. These weak frame (corresponding to water-saturated media) and stiff frame (air-saturated media) limits have been previously examined by Geertsma and Smit[18] and by Johnson and Plona.[19]

Biot's theory is briefly outlined in the next section. Plane wave solutions are then derived, and the relationship between the fluid and solid motions are investigated. Section III discusses the reflection and transmission of plane waves across a fluid/porous solid interface. Here, major differences between water- and air-filled media are found, which justify the quite different approaches sometimes used to perform approximate calculations for the two cases. A summary follows.

II. SUMMARY OF BIOT'S THEORY

A. Equations of motion

With reference to a right-handed Cartesian coordinate system, letting $\mathbf{u}$ represent the displacement of the solid frame, $\mathbf{U}$ the displacement of the fluid, Ω the porosity, and $\mathbf{w}=\Omega(\mathbf{u}-\mathbf{U})$ the fluid displacement relative to the frame, Biot[3] derived the constitutive equations

$$\sigma_{ij}=2\mu e_{ij}+[(H-2\mu)e-C\zeta]\delta_{ij}, \tag{1}$$

[a)]An earlier version of this article was presented at the 120th Meeting of the Acoustical Society of America, San Diego, CA, 26–30 November, 1990. J. Acoust. Soc. Am. **88**. S121 (1990).

where σ_{ij} are the components of stress, e_{ij} are the components of the strain tensor, μ is the complex shear modulus of the skeletal frame, H and C are complex moduli, $e=\nabla\cdot\mathbf{u}$ is the volumetric strain of the solid, $\zeta=\nabla\cdot\mathbf{w}$ is the increment in fluid content, and δ_{ij} is the Kronecker delta. Comparing this stress-strain relation with that for an isotropic elastic medium

$$\sigma_{ij}=2\mu e_{ij}+\xi e\delta_{ij} \tag{2}$$

(where ξ is the Lamé parameter) shows that the forms are similar, with additional complex moduli introduced to describe the effect of the fluid-filled pores. Stoll and Bryan[20] give expressions for calculating values of the Biot moduli H and C (and M which appears below) from the bulk moduli of the solid and fluid components of the porous material and the frame bulk modulus (K_b). The values of the solid particle density ρ_s and solid particle bulk modulus K_s are required, along with the fluid density ρ_f, bulk modulus K_f, and kinematic viscosity ν. For the skeletal frame, the porosity Ω, zero-frequency permeability k_0, tortuosity α, shear modulus G, and Poisson's ratio n must be given. The frame bulk modulus K_b is then estimated using the relation $K_b=G[(2/3)+2n/(1-2n)]$. Johnson *et al.*[21] showed that these parameters can be measured independently, and that Biot's theory then correctly predicts the acoustic behavior of porous materials.

Viscoelastic losses are incorporated in the theory by specifying a value for the loss decrement δ, and by replacing, e.g., the shear modulus by a complex modulus $\mu=G(1+i\delta)$, where $i=(-1)^{1/2}$. In this poroviscoelastic model, all of the moduli become complex and frequency dependent.[22]

Using the constitutive Eq. (1), Biot derived the coupled equations of motion

$$\mu\nabla^2\mathbf{u}+(H-\mu)\nabla e-C\nabla\zeta=\rho\partial_t^2\mathbf{u}-\rho_f\partial_t^2\mathbf{w}, \tag{3}$$

$$C\nabla e-M\nabla\zeta=\rho_f\partial_t^2\mathbf{u}-(\alpha\rho_f/\Omega)\partial_t^2\mathbf{w}-\frac{\rho_f\nu}{k_0}F(\omega)\partial_t\mathbf{w}, \tag{4}$$

where M is a complex modulus, ρ is the average density, and $F(\omega)$ is a frequency-dependent correction to the viscosity. In past work, simple pore geometries (e.g., cylindrical tubes or slits) have been assumed, and analytical expressions for have been derived and used for $F(\omega)$.[1-12]

Recently, the theory of the dynamic response of a fluid in a porous medium has been advanced and generalized using the concepts of dynamic permeability and tortuosity.[23,24] Using this theory and assuming $e^{i\omega t}$ time dependence, Eq. (4) becomes

$$C\nabla e-M\nabla\zeta=\rho_f\partial_t^2\mathbf{u}-[\rho_f\tilde{\alpha}(\omega)/\Omega]\partial_t^2\mathbf{w}=\rho_f\partial_t^2\mathbf{u}-m'\partial_t^2\mathbf{w}, \tag{5}$$

with $m'=\rho_f\tilde{\alpha}(\omega)/\Omega=(\rho_f/\Omega)[\alpha_\infty^2-i\eta\Omega F(\omega)/(\rho_f k_0\omega)]$, and where $\tilde{\alpha}(\omega)$ is the dynamic tortuosity given by

$$\tilde{\alpha}(\omega)=\alpha-i(\eta\Omega/\omega k_0\rho_f)F(\omega)=\alpha[1-i(\omega/\omega_c)F(\omega)], \tag{6}$$

and $F(\omega)$ is

$$F(\omega)=[1+i(4\alpha_\infty^2k_s^2\rho_f\omega/\eta\Omega^2\Lambda^2)]^{1/2}=[1+i\tfrac{1}{2}N(\omega/\omega_c)]^{1/2}. \tag{7}$$

In the above equations, the dynamic viscosity of the fluid is represented by $\eta=\rho_f\nu$. Also, a parameter $N=8\alpha k_0/(\Omega\Lambda^2)$ has been introduced, along with a characteristic frequency[25] $\omega_c=\eta\Omega/(\rho_f k_0\alpha)$; the frequency at which the viscous skin depth becomes about equal to the pore size. For frequencies below ω_c, viscous effects dominate the flow in the porous medium, while for frequencies above ω_c, inertial effects are more important. The characteristic length Λ can be determined from a flow-velocity weighted pore-volume-to-surface ratio [see Eq. (2.17) of Ref. 23]. For smoothly varying pore geometries, the dynamic tortuosity can be accurately represented by the scaled analytical solution for a cylindrical tube.[23-29] For most porous media, $N\approx 1$, the value assumed here.[23,27]

For air-saturated porous materials, temperature effects cause the fluid bulk modulus to be frequency dependent, and Champoux and Allard[30] have derived expressions accounting for these effects, which have been incorporated into the calculations presented here.

B. Propagation of plane waves

The solid and fluid displacements can be represented by scalar and vector potentials

$$\mathbf{u}=\nabla\phi_s+\nabla\times\psi_s, \tag{8}$$

$$\mathbf{w}=\nabla\phi_f+\nabla\times\psi_f, \tag{9}$$

with $\psi=(0,\psi,0)$. We first examine curl-free motion by setting the ψ terms to zero and substitute these potentials into Eqs. (3) and (5). This process leads to the coupled wave equations

$$H\nabla^2\phi_s-C\nabla^2\phi_f=\rho\partial_t^2\phi_s-\rho_f\partial_t^2\phi_f, \tag{10}$$

$$C\nabla^2\phi_s-M\nabla^2\phi_f=\rho_f\partial_t^2\phi_s-m'\partial_t^2\phi_f. \tag{11}$$

Next, by substituting in the plane wave potentials $\phi_s=A_i\exp[i(\omega t-\mathbf{k}\cdot\mathbf{r})]$ and $\phi_f=B_i\exp[i(\omega t-\mathbf{k}\cdot\mathbf{r})]$, Eqs. (10) and (11) reduce to

$$\begin{bmatrix} Hk^2-\rho\omega^2 & \rho_f\omega^2-Ck^2 \\ Ck^2-\rho_f\omega^2 & m'\omega^2-Mk^2 \end{bmatrix}\begin{bmatrix}\phi_s\\ \phi_f\end{bmatrix}=\begin{bmatrix}0\\0\end{bmatrix}. \tag{12}$$

This system of equations has solutions when the determinant of the 2×2 matrix is zero. Writing out this determinant leads to a quadratic expression in $k^2=\mathbf{k}\cdot\mathbf{k}$, which has two solutions for the complex wave number $\mathbf{k}$. This result

TABLE I. Input parameters used in the calculations, and derived properties of the porous media.

Input parameters for sand			
Density of solid grains	ρ_s(kg m^{-3})	2650	
Bulk modulus of solid grains	K_s (Pa)	3.6×10^{10}	
Shear modulus of frame	μ (Pa)	5×10^{7}	
Poisson's ratio	n	0.33	
Porosity	Ω	0.3	
Permeability	k_0 (m^2)	1×10^{-10}	
Loss decrement	δ	0.02	
Tortuosity	α	1.25	
Input parameters for the fluids		**Water**	**Air**
Density	ρ_f (kg m^{-3})	1000	1.2
Bulk modulus	K_f (Pa)	2.3×10^{9}	1.3×10^{5}
Kinematic viscosity	ν (m^2 s^{-1})	1×10^{-6}	1.45×10^{-5}
Calculated properties of the porous media		**Sand/water**	**Sand/air**
Density	ρ(kg m^{-3})	2155	1855
Bulk modulus of frame	K_b (Pa)	1.3×10^{8}	1.3×10^{8}
P_1 wave velocity	Re(v_1) (m s^{-1})	1911	328
S wave velocity	Re(v_3) (m s^{-1})	152	164
Critical frequency	$f_c=\omega_c/2\pi$ (Hz)	380	5540

shows that there are two propagating compressional waves, with different propagation velocities, that are termed compressional waves of the first and second kinds and are denoted by P_1 and P_2. Plona[31] experimentally confirmed Biot's theory by observing the two predicted compressional waves. Yamamoto[8] [Eq. (10)] gives explicit expressions for these wave velocities. The wavenumbers for the two compressional waves, k_1 and k_2, are given by the expression

$$k_{1,2}^2=\omega^2\frac{\{-(m'H+\rho M-2\rho_f C)\pm[(m'H-\rho M)^2+4(\rho_f H-m'C)(\rho_f M-m'C)]^{1/2}\}}{2(C^2-HM)}. \tag{13}$$

Setting the scalar potentials ϕ to zero in Eqs. (8) and (9), substituting into Eqs. (3) and (5), and substituting plane wave potentials for ψ leads to

$$\begin{bmatrix}\omega^2\rho-\mu k_3^2 & -\omega^2\rho_f\\ \omega^2\rho & -\omega^2 m'\end{bmatrix}\begin{bmatrix}\psi_s\\ \psi_f\end{bmatrix}=\begin{bmatrix}0\\0\end{bmatrix}, \tag{14}$$

where the subscript 3 is used to identify shear wave parameters. Setting the determinant of the matrix to zero leads to a linear equation in k_3^2, with a single solution

$$k_3^2=[1-(\rho_f^2/\rho m')]\omega^2\rho/\mu. \tag{15}$$

Displacements induced in the solid and fluid phases of the porous medium are coupled to one another, i.e., a disturbance propagating in the solid matrix induces a displacement in the pore fluid (even for shear waves), and similarly a disturbance in the pore fluid induces one in the solid matrix. The relation between the motion in the solid and fluid phases is related to the displacement potential ratios (B_i/A_i) for the compressional and shear waves. These ratios can be derived by substituting the plane wave potentials into the wave equations and leads to the expressions

$$B_i/A_i=(H|k_i|^2-\rho\omega^2)/(C|k_i|^2-\rho_f\omega^2),\quad i=1,2, \tag{16}$$

for the two compressional waves and

$$B_3/A_3=(\rho/\rho_f)-(\mu|k_3|^2/\rho_f\omega^2) \tag{17}$$

for the shear waves. Using Eqs. (16) and (17), the fluid to solid displacement amplitude ratios can be calculated from the expression

$$U/u=1-[B/(\Omega A)]. \tag{18}$$

To investigate the differences between wave propagation in water- and air-filled porous media, the predicted wave propagation characteristics of sand are calculated. The physical parameters used in these calculations are given in Table I; the values for sand and sea water were taken from Yamamoto.[9]

Figure 1 (top) shows the predicted velocity of the three wave types (P_1, P_2, and S) in water-filled sand as a function of frequency. Both the P_1 and S wave speeds are essentially independent of frequency. The velocity of the P_2 wave is less than that of the P_1 wave, so these waves are sometimes called the slow and fast compressional waves, respectively. The P_2 wave velocity increases as the fre-

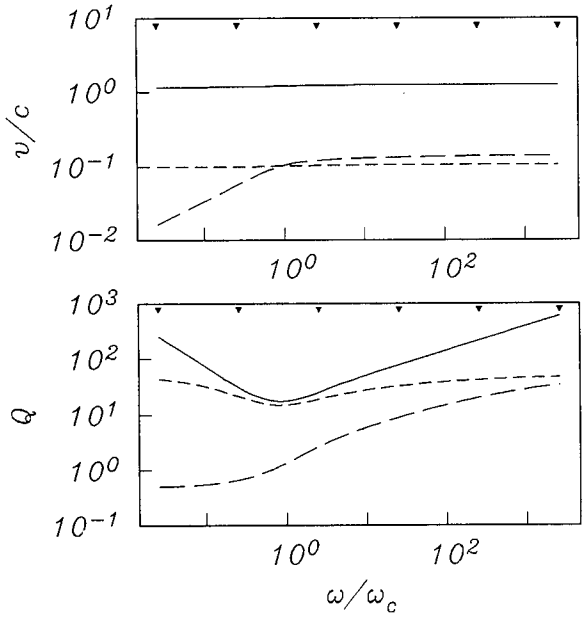

FIG. 1. Velocity and attenuation predicted by the Biot theory for the three types of waves in water-filled sand. The assumed sand and water properties were taken from Yamamoto (see Ref. 9) and are listed in Table I. Solid lines are plotted for the P_1 (fast compressional) wave, long dashed lines for the P_2 (slow compressional) wave, and short dashed lines for the S (shear) wave. Small triangles mark the frequencies 10, 10^2, 10^3, 10^4, 10^5, and 10^6 Hz. (Top) Velocity normalized by the fluid velocity $c=1517$ m s^{-1} as a function of the normalized frequency ω/ω_c. (Bottom) Dimensionless attenuation parameter Q as a function of frequency.

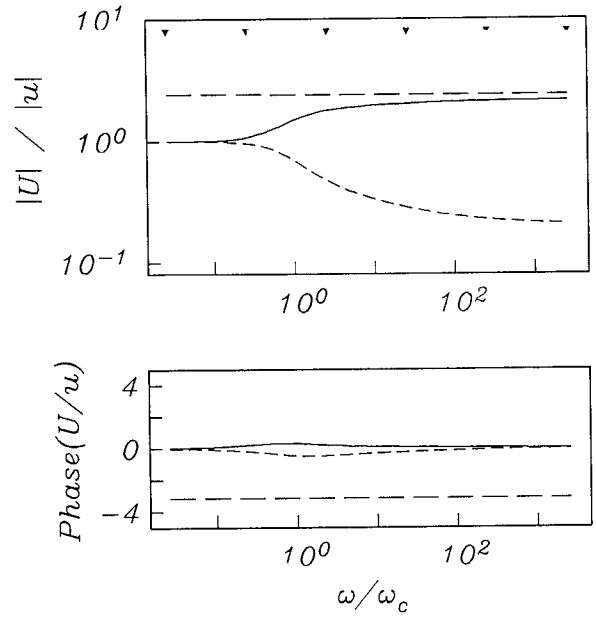

FIG. 2. Fluid/solid displacement ratios predicted by the Biot theory for the three waves in a water-filled sand. Same lines assignments as in Fig. 1. (Top) Amplitude ratios. (Bottom) Phase of the ratios in radians. A positive phase corresponds to the fluid motion lagging behind the solid motion.

quency increases until $\omega\approx\omega_c$ ($f\approx400$ Hz), after which it remains constant and slightly greater than the S wave velocity as the frequency increases.

The wave attenuations are also shown in Fig. 1 (bottom) in terms of the quality factor $Q=\text{Real}(v)/[2\,\text{Imag}(v)]$, where v is the phase velocity. If Q is constant with respect to frequency, a situation commonly assumed in seismology, then the losses are also constant with respect to wavelength and the spatial attenuation constant β, in the term $e^{-\beta r}$, increases as f increases. For the P_1 and S waves, the attenuation maxima occur near $\omega\approx\omega_c$ (where Q is a minimum). For the P_2 wave, the attenuation is very large at low frequencies, decreases to a value of $Q=1$ at about $\omega\approx\omega_c$, and continues to decrease as the frequency increases. Values of Q less than 1 imply that the wave is not a true propagating wave because the attenuation is so large; it is a diffusion at these frequencies. The value $\omega\approx\omega_c$ is where the viscous drag and the inertial losses are approximately equivalent, and where the P_2 wave becomes a propagating rather than a diffusive wave.

As Yamamoto[9] points out, the general behavior of the material remains the same if the permeability k_0 changes. Although changing k_0 causes a shift in frequency, the velocities and attenuations remain constant at constant ω/ω_c.

Figure 2 shows the ratio of the fluid to solid displacement amplitudes calculated using Eqs. (16)–(18) for the three wave types in the water-filled sand. For P_1 and S waves, the fluid/solid displacement ratios (U/u) are equal at low frequencies. As the frequency increases beyond $0.1\omega_c$, the fluid displacement amplitude increases for the P_1 wave, becoming twice as large as the solid displacement at high frequencies. For the shear wave, the fluid displacement decreases to about $\frac{1}{5}$ of the solid displacement. For both of these waves, the fluid and solid motions remain in phase, except for a slight deviation near ω_c, where the fluid motion leads the solid (by about 18°) for the P_1 wave, and lags behind (by about 30°) for the shear wave. The ratio for the P_2 wave is nearly constant and has a value of 2.4. For this wave the fluid and solid components of motion are 180° out of phase.

Figure 3 shows the predicted velocities and attenuations for the three wave types for the same sand, but air filled rather than water filled. Table I gives the values used for air. Once again, the P_1 and S wave velocities are essentially constant with respect to frequency. The P_2 velocity again increases with frequency, but approaches the P_1 velocity (not the S velocity as in the previous example) at high frequencies. The P_1 and S waves are not affected by viscous attenuation, as Q is constant for these waves, implying that β is proportional to f. The slow wave is very highly attenuated at low frequencies, and less attenuated above $\omega\approx\omega_c$, where it becomes a true propagating wave. One consequence of replacing the water with air is to shift the "critical" value of $\omega\approx\omega_c$ to a much higher frequency (5.5 kHz), because of the higher kinematic viscosity for air.

The fluid/solid displacement ratios for the air-filled sand are shown in Fig. 4. The behavior of these ratios as a function of frequency is similar to that of water-filled sand.

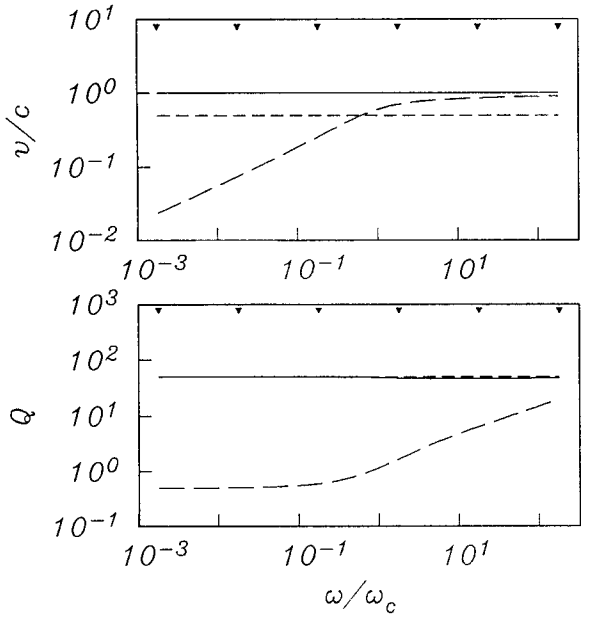

FIG. 3. Velocity and attenuation predicted by the Biot theory for the three types of waves in air-filled sand. The assumed sand properties are the same as for the previous example (taken from Yamamoto, see Ref. 9), and are listed along with the air properties in Table I. Same line assignments as in Fig. 1. Small triangles mark the frequencies 10, 10^2, 10^3, 10^4, 10^5, and 10^6 Hz. (Top) Velocity normalized by the fluid velocity $c=329$ m s^{-1} as a function of the normalized frequency ω/ω_c. (Bottom) Dimensionless attenuation parameter Q as a function of frequency.

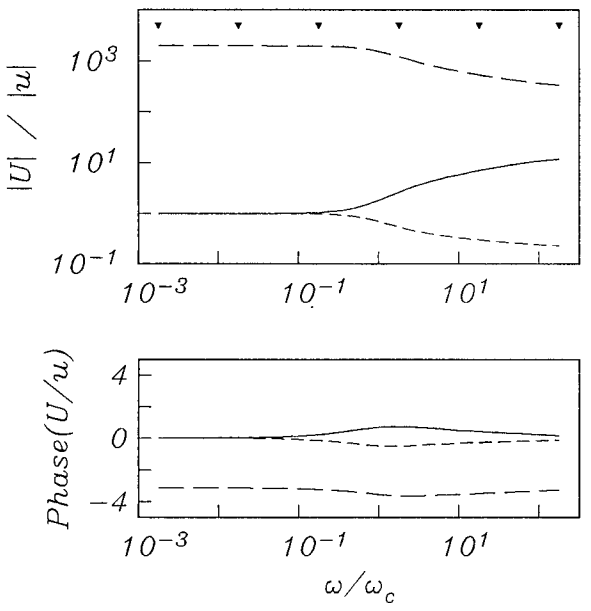

FIG. 4. Fluid/solid displacement ratios predicted by the Biot theory for the three waves in a air-filled sand. Same line assignments as in Fig. 1. (Top) Amplitude ratios. (Bottom) Phase of the ratios in radians. A positive phase corresponds to the fluid motion lagging behind the solid motion.

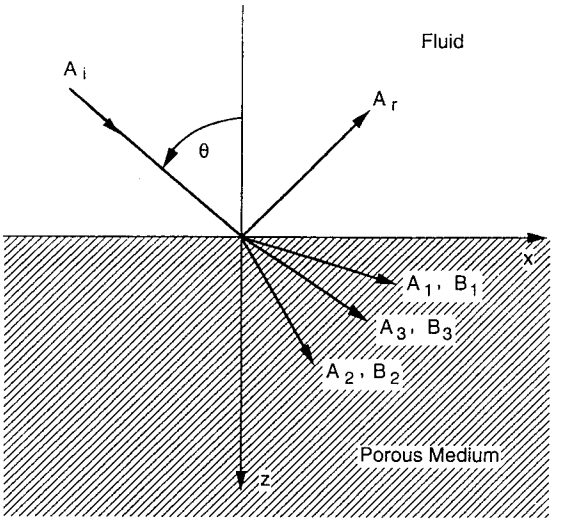

FIG. 5. A plane compressional wave incident from a fluid onto a fluid-saturated porous medium. The displacement potential amplitudes for each of the waves are indicated on the figure. Subscripts i and r denote the incident and reflected waves in the fluid; subscripts 1, 2, and 3 refer to the fast compressional, slow compressional, and shear waves in the porous solid. θ is the angle of incidence.

The major difference is that the ratio is now ~ 2000 for the P_2 wave, compared to 2.4 when the sand was water filled. Thus, this wave propagates mainly through the pores, as if the solid were rigid, when the sand is air-filled. The P_2 wave is still coupled to the solid as its high attenuation shows. There is also a decrease in the ratio for P_2 waves to ~ 340 as ω/ω_c increases beyond 1. The phase behavior of the ratio for all three waves is similar to the behavior found for the water-filled sand, with the P_1 and shear wave motions in phase and the P_2 motions out of phase. At $\omega \approx \omega_c$, the P_1 fluid motion leads the solid motion by nearly 45°, while the shear and P_2 waves have phase lags of around 30°.

III. REFLECTION AND TRANSMISSION OF PLANE WAVES AT A FLUID/POROUS SOLID INTERFACE

In this section, the interaction of a plane wave incident from a fluid onto a porous solid is investigated (Fig. 5). Deresiewicz and Skalak[32] were apparently the first to discuss the boundary conditions at an interface. Following Stoll and Kan,[7] we introduce wave potentials and write the boundary conditions in terms of them. In the fluid, we assume a downgoing compressional wave at an angle of θ from the vertical. The wavenumber in the fluid is $k_f=\omega/c$, with c the velocity in the fluid, and the vertical and horizontal wavenumbers are $k_z=k_f\cos\theta$ and $k_x=k_f\sin\theta$. The incident and reflected wave potentials in the fluid are

$$\phi_i=A_i\exp[i(\omega t-k_f\cos\theta\cdot z-k_x x)], \tag{19}$$

$$\phi_r=A_r\exp[i(\omega t+k_f\cos\theta\cdot z-k_x x)], \tag{20}$$

while in the porous material, the potentials are

$$\phi_s = A_1 \exp[i(\omega t - k_{1z} z - k_x x)] + A_2 \exp[i(\omega t - k_{2z} z - k_x x)], \quad (21)$$

$$\phi_f = B_1 \exp[i(\omega t - k_{1z} z - k_x x)] + B_2 \exp[i(\omega t - k_{2z} z - k_x x)], \quad (22)$$

$$\psi_s = A_3 \exp[i(\omega t - k_{3z} z - k_x x)], \quad (23)$$

$$\psi_f = B_3 \exp[i(\omega t - k_{3z} z - k_x x)]. \quad (24)$$

Here, the subscripts 1, 2, and 3 stand for the P_1, P_2, and S waves with solid motion potential amplitudes A_i, fluid motion potential amplitudes B_i, and vertical wavenumbers k_{iz}. Phase continuity in accordance with Snell's law is incorporated in the above expressions, so the horizontal wavenumbers for all of the waves are equal (k_x).

The boundary conditions for the fluid/solid interface are the continuity of normal fluid displacement, normal traction, fluid pressure, and tangential traction. These boundary conditions are written in matrix form as

$$A_i \begin{pmatrix} k_f \cos\theta \\ -\rho_f \omega^2 \\ -\rho_f \omega^2 \\ 0 \end{pmatrix} = \begin{bmatrix} k_f \cos\theta & k_{1z}\left(1-\frac{B_1}{A_1}\right) & k_{2z}\left(1-\frac{B_2}{A_2}\right) & k_x\left(1-\frac{B_3}{A_3}\right) \\ \rho_f \omega^2 & \left(\frac{B_1}{A_1}C-H\right)(k_x^2+k_{1z}^2)+2\mu k_x^2 & \left(\frac{B_2}{A_2}C-H\right)(k_x^2+k_{2z}^2)+2\mu k_x^2 & -2\mu k_x k_{3z} \\ \rho_f \omega^2 & \left(\frac{B_1}{A_1}M-C\right)(k_x^2+k_{1z}^2) & \left(\frac{B_2}{A_2}M-C\right)(k_x^2+k_{2z}^2) & 0 \\ 0 & 2k_x k_{1z} & 2k_x k_{2z} & k_x^2-k_{3z}^2 \end{bmatrix} \times \begin{pmatrix} A_r \\ A_1 \\ A_2 \\ A_3 \end{pmatrix} \quad (25)$$

and are solved numerically using LINPACK subroutines.[33]

Dutta and Ode[34] have presented a clear discussion of the energy partitioning at a boundary between two porous media, and were the first to point out the existence of interference fluxes of energy between the three types of waves. Energy coefficients for water-saturated porous materials have also been calculated by Wu *et al.*[35] Following Dutta and Ode's[34] development, the energy reflection and transmission coefficients are defined as

$$R = F_R / F_I, \quad (26)$$

$$T_{ii} = F_{ii} / F_I, \quad i = 1,2,3, \quad (27)$$

where the z component of the energy fluxes are defined as

$$F_I = \left(\frac{\omega}{2\pi}\right) \int_0^{2\pi/\omega} \mathrm{Re}(p_I)\mathrm{Re}(\dot{U}_{zI})\,dt \quad (28)$$

for the incident wave in the fluid,

$$F_R = \left(\frac{\omega}{2\pi}\right) \int_0^{2\pi/\omega} \mathrm{Re}(p_r)\mathrm{Re}(\dot{U}_{zr})\,dt \quad (29)$$

for the reflected wave in the fluid, and

$$F_{ii} = \left(\frac{\omega}{2\pi}\right) \int_0^{2\pi/\omega} [\mathrm{Re}(\sigma_{xzi})\mathrm{Re}(\dot{u}_{xi}) + \mathrm{Re}(\sigma_{zzi})\mathrm{Re}(\dot{u}_{zi}) + \mathrm{Re}(p_i)\mathrm{Re}(\dot{w}_{zi})]\,dt, \quad i = 1,2,3, \quad (30)$$

for the waves in the porous medium. The interference fluxes are defined as

$$F_{ij} = \left(\frac{\omega}{2\pi}\right) \int_0^{2\pi/\omega} [\mathrm{Re}(\sigma_{xzi})\mathrm{Re}(\dot{u}_{xj}) + \mathrm{Re}(\sigma_{zzi})\mathrm{Re}(\dot{u}_{zj}) + \mathrm{Re}(\sigma_{xzj})\mathrm{Re}(\dot{u}_{xi}) + \mathrm{Re}(\sigma_{zzj})\mathrm{Re}(\dot{u}_{zi}) + \mathrm{Re}(p_i)\mathrm{Re}(\dot{w}_{zj}) + \mathrm{Re}(p_j)\mathrm{Re}(\dot{w}_{zi})]\,dt, \quad i = 1,2,3. \quad (31)$$

With these definitions, the energy balance across the interface is expressed as

$$1 - R = T_{11} + T_{22} + T_{33} + T_{12} + T_{13} + T_{23}. \quad (32)$$

Figures 6 and 7 show three-dimensional views of the energy coefficients for the water- and air-filled sands as a function of incident angle and frequency. For the water/water-saturated sand boundary, all of the coefficients, except for transmission to the slow compressional P_2 wave, show only slight variations with frequency (Fig. 6). The reflection coefficient is about 0.2 at normal incidence and increases to 1.0 at grazing incidence, where all of the transmission coefficients decrease to zero. The transmission coefficient into P_1 (fast compressional) waves is around 0.8 at low angles of incidence and is always two or three orders of magnitude larger than the other two transmission coefficients. Transmission into P_2 waves is the only conversion that shows a large frequency dependence. At normal incidence, this coefficient increases by a factor of 4 from 10 to 10^5 Hz, while the shear wave transmission coefficient is always zero. From this figure, we see that nearly all of the

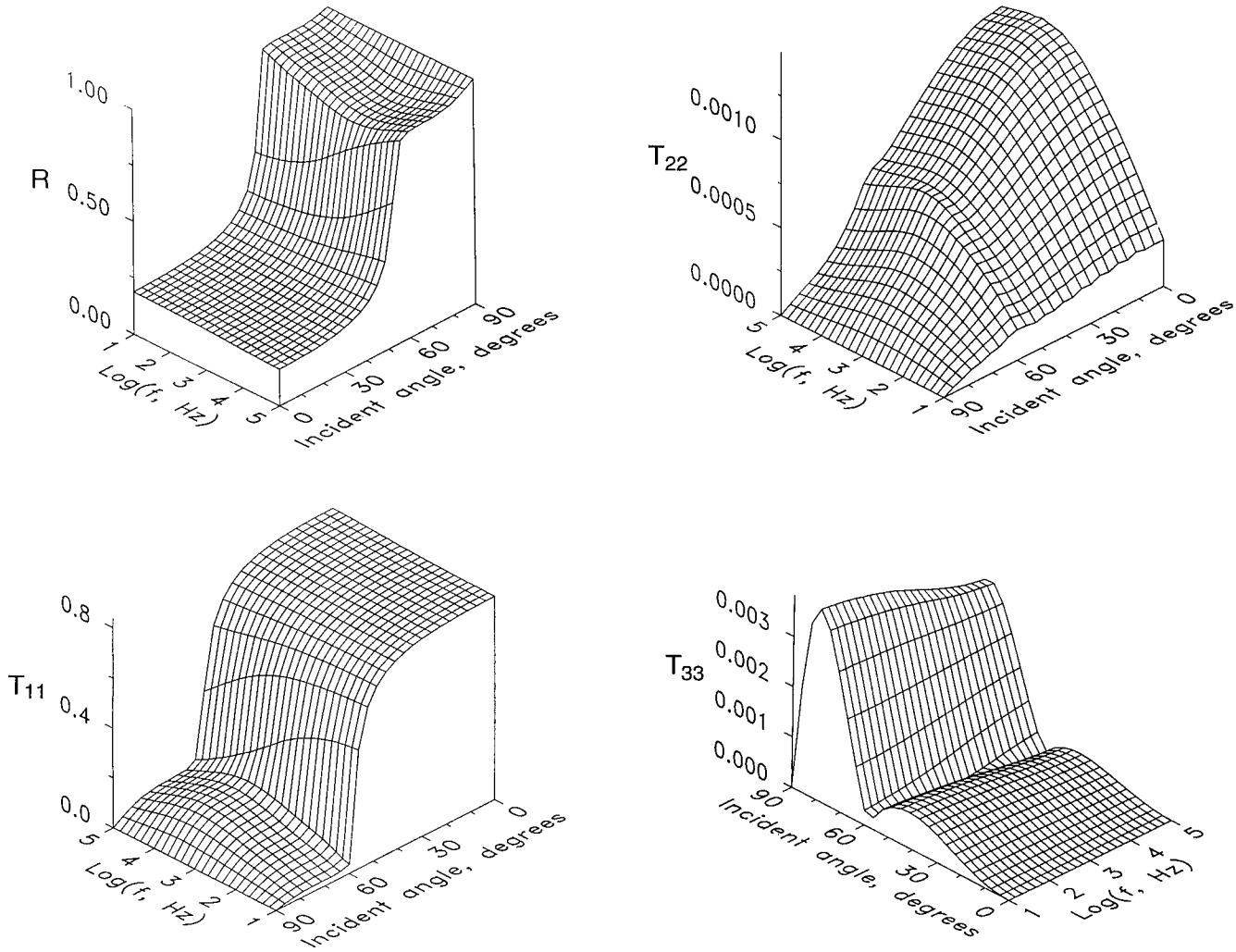

FIG. 6. Three-dimensional view of the reflected and transmitted energy coefficients for a plane wave incident on a water/water-filled sand interface. 0° corresponds to an angle of incidence normal to the fluid/porous solid boundary. The frequency axis is logarithmic, with a range from 10 to 10^5 Hz. (a) shows the ratio R of the vertical energy flux in the reflected wave to the vertical energy flux in the incident wave in the fluid, (b) shows the energy flux ratio T_{11} for the transmitted P_1 wave, (c) shows the energy flux ratio T_{22} for the transmitted P_2 wave, and (d) shows the energy flux ratio T_{33} for the transmitted S wave. Note that some of the displays have been rotated to give a clear view of the surface.

transmitted energy is converted into P_1 waves in the porous solid, with only minute amounts ($<0.5\%$) converted into P_2 or S waves. The only significant frequency dependence resides in a coefficient that is always small, so the overall response is essentially independent of frequency.

Figure 7 shows the energy coefficients for a plane wave in air incident upon a boundary with air-filled sand, and there are two major differences in comparison with the previous case where water was the fluid. First, all of the coefficients exhibit some frequency dependence. The P_2 transmission coefficient still increases with frequency, but now the reflected and S transmission coefficients decrease with frequency. The reflection coefficient decreases from nearly 1.0 at 10 Hz to about 0.4 at 10^5 Hz for normal incidence. The second difference is that the P_2 transmission coefficient is now the largest, not the P_1. The P_1 and S waves account for at most 2.3% and usually less than 1% of the energy incident upon the boundary. For air-filled sand, most of the transmitted energy will be converted into P_2 waves, not P_1 waves as was the case for water-filled sand.

These examples show why quite different approximations can be used to treat reflections from the fluid/porous solid boundary in underwater and aeroacoustics. For water-filled porous materials, the P_2 wave can often be ignored, since it is of small amplitude. The main effect of the pores is on the P_1 and S wave attenuations (see Fig. 1), and if these are calculated according to the Biot theory, accurate results can be obtained for some undersea sediments.[10] For air-filled materials, it is the P_2 (slow compressional) wave that is most important, and a rigid porous model, ignoring the P_1 and S waves, has found wide application in this situation.[13,17,36] If motion induced in the porous medium is of interest, however, the full Biot treatment will need to be used. Even for air-filled materials, the P_1 wave will become significant as the distance from the interface into the porous medium increases because of the high P_2 wave's attenuation rate.

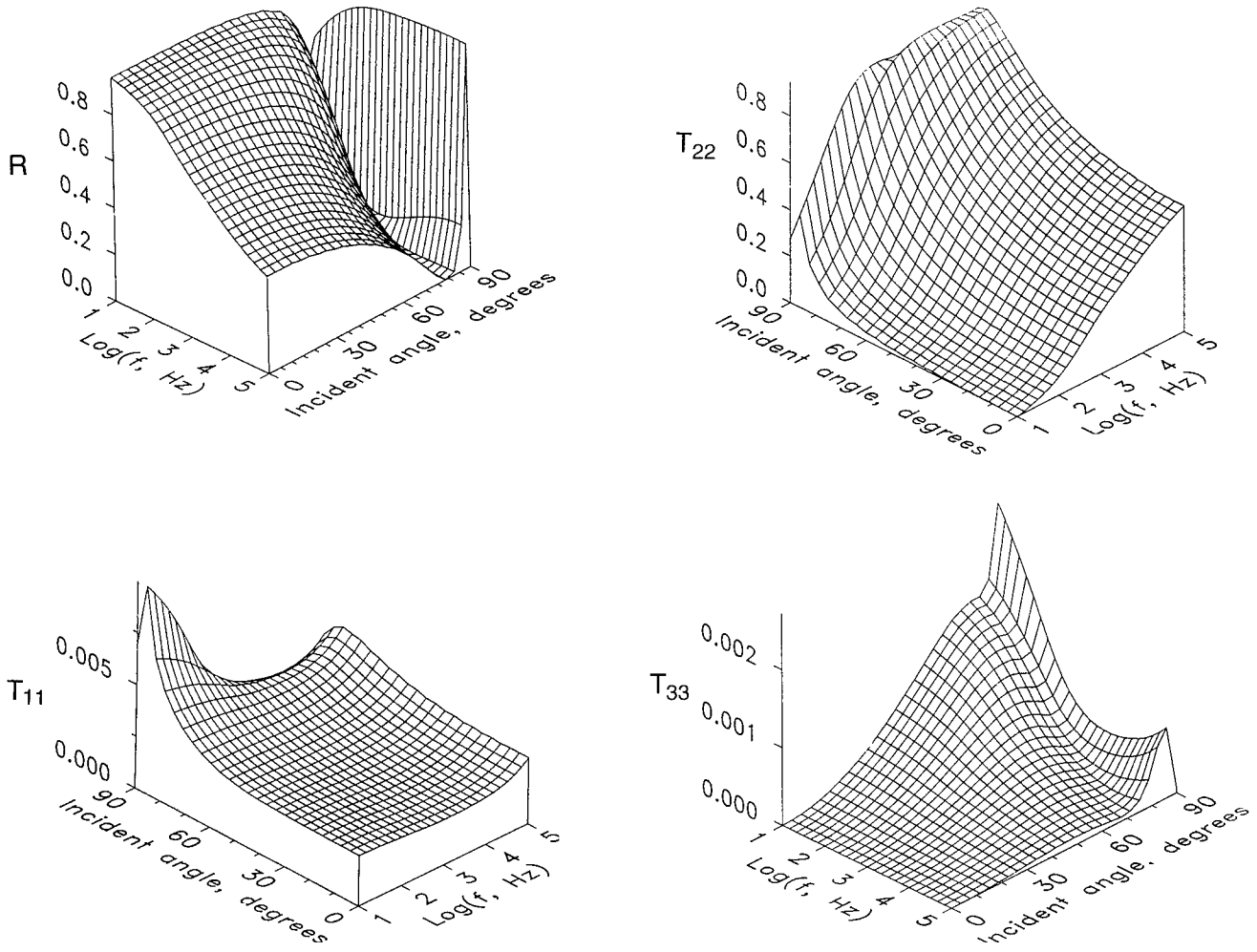

FIG. 7. Three-dimensional view of the energy reflection and transmission coefficients for plane wave incident on an air/air-filled sand interface. (a)–(d) show coefficients for the reflected and for the transmitted P_1, P_2, and S waves, respectively. Note that some of the displays have been rotated to give a clear view of the surface.

IV. CONCLUDING REMARKS

Calculations using Biot's theory have been used to investigate differences between water- and air-filled porous materials. These calculations show that both materials have P_1 and S wave velocities that are essentially frequency independent, with a P_2 velocity that increases at low frequencies and levels off at a constant value at high frequencies. The fast and shear wave attenuations have some frequency dependence for water-filled sand but are constant for air-filled sand, while the slow compressional wave attenuation decreases with frequency for both materials. The slow compressional wave's fluid/solid coupling coefficient is around 2 for water-filled materials, but greater than 300 for air-filled materials, implying that the wave motion is decoupled from the solid when the saturating fluid is air.

Major differences were found for plane wave transmission into the two types of porous materials. For water-filled media, transmission to P_1 waves is the most important, while for air-filled media, transmission to P_2 waves is the largest. These differences naturally lead to quite different approximation methods for the two cases.

Additional experimental work is planned to confirm these calculations. Sonic velocity and attenuation measurements on various porous materials as a function of frequency are planned in conjunction with permeability measurements; these measurements will be used to validate these calculations.

ACKNOWLEDGMENTS

Steve Arcone and Jerry Johnson of CRREL provided helpful reviews of this article, and Steve Tooms, of the Open University, Milton Keynes, UK, independently confirmed the displacement ratio calculations. This work was supported by the Directorate of Research and Development, U.S. Army Corps of Engineers, DA Project 4A161102AT24.

[1] M. A. Biot, J. Acoust. Soc. Am. **28**, 168 (1956).
[2] M. A. Biot, J. Acoust. Soc. Am. **28**, 179 (1956).
[3] M. A. Biot, J. Appl. Phys. **33**, 1482 (1962).
[4] R. D. Stoll, *Physics of Sound in Marine Sediments,* edited by L. Hampton (Plenum, New York, 1974), pp. 19–39.
[5] R. D. Stoll, Geophysics **42**, 715 (1977).

[6] R. D. Stoll, J. Acoust. Soc. Am. **68**, 1341 (1980).
[7] R. D. Stoll and T. -K. Kan, J. Acoust. Soc. Am. **77**, 149 (1981).
[8] T. Yamamoto, Bull. Seism. Soc. Am. **73**, 1599 (1983).
[9] T. Yamamoto, J. Acoust. Soc. Am. **73**, 1587 (1983).
[10] T. Yamamoto, *Acoustics and the Sea-Bed*, edited by N. G. Pace (Bath University Press, Bath, UK, 1983), pp. 279–287.
[11] M. Badiey and T. Yamamoto, J. Acoust. Soc. Am. **77**, 954 (1985).
[12] K. Attenborough, J. Acoust. Soc. Am. **73**, 785 (1983).
[13] K. Attenborough, J. Sound Vibration **99**, 521 (1985).
[14] K. Attenborough, J. Acoust. Soc. Am. **81**, 93 (1987).
[15] K. Attenborough and T. L. Richards, J. Acoust. Soc. Am. **86**, 1085 (1989).
[16] K. Attenborough, J. M. Sabatier, H. E. Bass, and L. N. Bolen, J. Acoust. Soc. Am. **79**, 1353 (1986).
[17] J. M. Sabatier, H. E. Bass, L. N. Bolen, K. Attenborough, and V. V. S. S. Sastry, J. Acoust. Soc. Am. **79**, 1345 (1986).
[18] J. Geertsma and D. C. Smit, Geophysics **26**, 169 (1961).
[19] D. L. Johnson and T. J. Plona, J. Acoust. Soc. Am. **72**, 556 (1982).
[20] R. D. Stoll and G. M. Bryan, J. Acoust. Soc. Am. **47**, 1440 (1970).
[21] D. L. Johnson, T. J. Plona, C. Scala, F. Pasierb, and H. Kojima, Phys. Rev. Lett. **49**, 1840 (1982).
[22] P. N. J. Rasolofosaon, J. Acoust. Soc. Am. **89**, 1532 (1991).
[23] D. L. Johnson, J. Koplik, and R. Dashen, J. Fluid. Mech. **176**, 379 (1987).
[24] D. L. Johnson, J. Koplik, and L. M. Schwartz, Phys. Rev. Lett. **57**, 2564 (1986).
[25] P. Sheng and M. -Y. Zhou, Phys. Rev. Lett. **61**, 1591 (1988).
[26] E. Charlaix, A. P. Kushnick, and J. P. Stokes, Phys. Rev. Lett. **61**, 1595 (1988).
[27] D. L. Johnson, Phys. Rev. Lett. **63**, 580 (1989).
[28] P. Sheng, M. -Y. Zhou, E. Charlaix, A. P. Kushnick, and J. P. Stokes, Phys. Rev. Lett. **63**, 581 (1989).
[29] M. -Y. Zhou and P. Sheng, Phys. Rev. B **39**, 12 027 (1989).
[30] Y. Champoux and J. -F. Allard, J. Appl. Phys. **70**, 1975 (1991).
[31] T. J. Plona, Appl. Phys. Lett. **36**, 259 (1980).
[32] H. Deresiewicz and R. Skalak, Bull. Seismol. Soc. Am. **53**, 783 (1963).
[33] J. J. Dongarra, J. R. Bunch, C. B. Molar, and G. W. Stewart, *LINPACK User's Guide* (SIAM, Philadelphia, 1979).
[34] N. C. Dutta and H. Odé, Geophysics **48**, 148 (1983).
[35] K. Xu, Q. Xue, and L. Adler, J. Acoust. Soc. Am. **87**, 2349 (1990).
[36] D. G. Albert and J. A. Orcutt, J. Acoust. Soc. Am. **87**, 93 (1990).